

Elastic gauge fields and zero-field 3D quantum Hall effect in hyperhoneycomb lattices

Sang Wook Kim and Bruno Uchoa

Department of Physics and astronomy, University of Oklahoma, Norman, Oklahoma 73019, USA

(Dated: November 29, 2021)

Dirac materials respond to lattice deformations as if the electrons were coupled to gauge fields. We derive the elastic gauge fields in the hyperhoneycomb lattice, a three dimensional (3D) structure with trigonally connected sites. In its semimetallic form, this lattice is a nodal-line semimetal with a closed loop of Dirac nodes. Using strain engineering, we find a whole family of strain deformations that create uniform nearly flat Landau levels in 3D. We propose that those Landau levels can be created and tuned in metamaterials with the application of a simple uniaxial temperature gradient. In the 3D quantum anomalous Hall phase, which is topological, we show that the components of the elastic Hall viscosity tensor are multiples of $\eta_H = \beta^2 \sqrt{3}/(8\pi a^3)$, where β is an elastic parameter and a is the lattice constant.

Introduction. In honeycomb lattices such as graphene [1], strain deformations couple to electronic degrees of freedom as gauge fields and can induce Landau level (LL) quantization with very large effective pseudomagnetic fields [2–5]. When the chemical potential is inside the gap of the LLs, the Hall conductivity per valley is quantized and the system is expected to show a zero-field quantum Hall effect (QHE). Due to the dispersion of the LLs, Hall conductivity quantization is not common in three dimensions (3D), and may occur only in extremely anisotropic systems such as Bechgaard salts [6, 7], Bernal graphite [8, 9], and in nodal-line semimetals [10–12]. Even in strongly anisotropic systems such as in nodal line semimetals, the physical implementation of the 3D QHE is challenging due to the unusual toroidal field geometry required [10]. With the help of strain engineering, one may in principle design 3D LLs with well defined gaps in between from real space configurations of magnetic field that would be otherwise impractical to realize.

In this Rapid communication, we derive the elastic gauge fields that follow from arbitrary lattice deformations in the hyperhoneycomb lattice, a natural 3D generalization of the honeycomb geometry where all sites are connected by coplanar trigonal bonds, as shown in Fig. 1a. In the semimetallic form, this lattice is an example of a nodal-line semimetal [10, 13–18]. We identify a whole family of lattice deformations that produce uniform nearly flat LLs in 3D, a prerequisite for the 3D zero-field QHE. We show that this family of non-trivial deformations can be physically implemented with the application of a simple temperature gradient along the axis perpendicular to the nodal line, leading to a tunable metal-insulator transition in the bulk. The strain deformations can be uniquely specified by the set of thermal expansion coefficients of the crystal. We propose that a tunable temperature controlled 3D zero-field QHE can be implemented in acoustic metamaterials [19].

In the presence of topological states, the topological invariants can manifest in the elastic response of the crystal through phonons. In the 3D quantum anomalous Hall (QAH) phase [20], which is the extension of the Haldane model [22] to the hyperhoneycomb lattice, we also calcu-

late the elastic Hall viscosity tensor $\eta_{\mu\nu\rho\gamma}$. Also known as the phonon Hall viscosity [23], this quantity is analogous to the dissipationless viscous response of electrons in the quantum Hall regime [25–27] and is topological in nature. We show that the components of the Hall viscosity tensor are $\pm\eta_H$ or $\pm 2\eta_H$ (or zero), with $\eta_H = \beta^2 \sqrt{3}/(8\pi a^3)$, where β is an elastic parameter and a is the lattice constant.

Hamiltonian. The hyperhoneycomb lattice has four sites per unit cell $\mu = 1, \dots, 4$ and is generated by the lattice vectors $\mathbf{a}_1 = (\sqrt{3}, 0, 0)$, $\mathbf{a}_2 = (0, \sqrt{3}, 0)$, and $\mathbf{a}_3 = (-\sqrt{3}/2, \sqrt{3}/2, 3)$, in units of the lattice constant a . In the momentum space, the reciprocal lattice is generated by the vectors $\mathbf{b}_1 = (2\pi/\sqrt{3}, 0, -\pi/3)$, $\mathbf{b}_2 = (0, -2\pi/\sqrt{3}, \pi/3)$ and $\mathbf{b}_3 = (0, 0, 2\pi/3)$, shown in Fig. 1b. The tight-binding Hamiltonian is a 4×4 matrix [10]

$$\mathcal{H}_{0,\mu\nu}(\mathbf{k}) = -t_0 \sum_{\vec{\delta}_{\mu\nu}} e^{i\mathbf{k} \cdot \vec{\delta}_{\mu\nu}}, \quad (1)$$

where t_0 is the hopping amplitude, $\vec{\delta}_{\mu\nu}$ are the nearest neighbor (NN) vectors between sites of species μ and ν and \mathbf{k} is the momentum measured from the center of

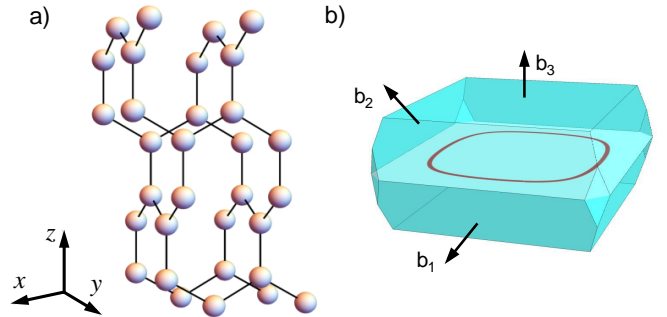


Figure 1. a) Hyperhoneycomb lattice, with four atoms per unit cell. All sites are linked by coplanar trigonal bonds spaced by 120° . b) Brillouin zone (BZ) of the hyperhoneycomb lattice, with the nodal line shown in red. The arrows show the reciprocal lattice vectors.

the Brillouin zone (BZ). In total, there are six NN vectors $\vec{\delta}_{12} = (\pm\sqrt{3}a/2, 0, a/2)$, $\vec{\delta}_{34} = (0, \pm\sqrt{3}a/2, a/2)$, $\vec{\delta}_{14} = (0, 0, -a)$ and $\vec{\delta}_{23} = (0, 0, a)$. The low energy bands of this lattice have a line of Dirac nodes $\mathbf{k}_0 = [k_x(s), k_y(s), 0]$ in the $k_z = 0$ plane, which can be written in terms of some parameter s that satisfies the equation $4 \cos[3k_x(s)/2] \cos[3k_y(s)/2] = 1$. The low energy projected Hamiltonian is described by a 2×2 matrix expanded around the nodal line

$$\mathcal{H}_{0,p}(\mathbf{q}) = [v_x(s)q_x + v_y(s)q_y] \sigma_1 + v_z(s)q_z \sigma_2 \quad (2)$$

where $\mathbf{q} \equiv \mathbf{k} - \mathbf{k}_0(s)$ is the relative momentum, σ_1, σ_2 are the two off-diagonal Pauli matrices and

$$\begin{aligned} v_x(s) &= \frac{\sqrt{3}}{1+\alpha^2} \sin\left(\frac{\sqrt{3}}{2}k_x(s)\right) t_0 \\ v_y(s) &= \frac{\alpha^2\sqrt{3}}{1+\alpha^2} \sin\left(\frac{\sqrt{3}}{2}k_y(s)\right) t_0 \\ v_z(s) &= -\frac{3\alpha}{1+\alpha^2} t_0, \end{aligned} \quad (3)$$

are the velocities of the quasiparticles, with $\alpha(s) \equiv 2 \cos[\sqrt{3}k_x(s)a/2]$ [20]. The energy spectrum of the quasiparticles is $E_0(\mathbf{q}) = \pm \sqrt{(v_x q_x + v_y q_y)^2 + v_z^2 q_z^2}$. The wavefunctions have a π Berry phase for closed line trajectories that encircle the nodal loop.

Elastic gauge fields. The inclusion of lattice deformations can be done by locally changing the distance between lattice sites, which affect value of the hopping constant. Expanding it to lowest order in the displacement of the lattice,

$$t(\vec{\delta}^{(n)} + \delta\mathbf{r}) \approx t_0 + \frac{\beta}{a^2} \delta_i^{(n)} \delta_j^{(n)} u_{ij} + \mathcal{O}(\delta r^2), \quad (4)$$

with $n = 1, \dots, 6$ indexing the 6 NN lattice vectors $\vec{\delta}^{(n)}$, $u_{ij} = \frac{1}{2}(\partial_i u_j + \partial_j u_i)$ is the strain tensor defined in terms of the displacement field \mathbf{u} of the lattice and $\beta = a \frac{\partial t}{\partial r} = \frac{\partial \log t}{\partial \log r}$ is the Grüneisen parameter of the model [21]. Including the lattice distortions in Hamiltonian (5), one gets two terms, $\mathcal{H}_p = \mathcal{H}_{0,p} + \mathcal{H}_{el}$, where

$$\mathcal{H}_{el} = \frac{3\beta}{4a} v_z (u_{xx} + u_{yy} - 2u_{zz}) \sigma_1 - \frac{\beta}{a} (v_x u_{xz} + v_y u_{yz}) \sigma_2 \quad (5)$$

is the elastic contribution. As in the 2D case (graphene), the deformation of the lattice couples to the Dirac fermions as an elastic gauge field \mathbf{A} . It is convenient to rewrite the Hamiltonian in the more familiar form

$$\mathcal{H}_p(\mathbf{q}) = [v_x (q_x + A_x) + v_y (q_y + A_y)] \sigma_1 + v_z (q_z + A_z) \sigma_2, \quad (6)$$

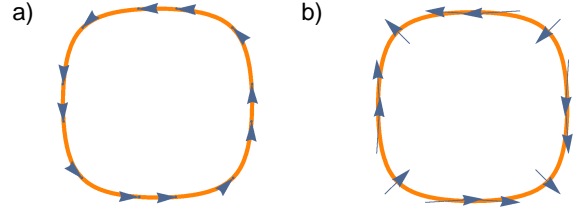


Figure 2. Pseudomagnetic field \mathbf{B} along the nodal line for two different strain field configurations. a) $\mathbf{u} = (2xz, 2yz, z^2)$ and b) $\mathbf{u} = (2yz, 2xz, 0)$. Both configurations lead to uniform \mathbf{B} fields in real space, but only the former produces nearly flat LLs.

where

$$\begin{aligned} A_x(s) &= \frac{v_x v_z}{v_\rho^2} \frac{3\beta}{4a} (u_{xx} + u_{yy} - 2u_{zz}) \\ A_y(s) &= \frac{v_y v_z}{v_\rho^2} \frac{3\beta}{4a} (u_{xx} + u_{yy} - 2u_{zz}) \\ A_z(s) &= -\frac{\beta}{a} \left(\frac{v_x}{v_z} u_{xz} + \frac{v_y}{v_z} u_{yz} \right) \end{aligned} \quad (7)$$

are the components of the elastic gauge field along the nodal line, with $v_\rho^2(s) = v_x^2(s) + v_y^2(s)$. The definition of the A_x and A_y components is to a degree arbitrary. In (7) we chose the most symmetric combination, although this choice has no effect in physical observables.

Those gauge fields can be associated to a pseudomagnetic field $\mathbf{B} = \nabla \times \mathbf{A}$, which follows from lattice deformations and hence must preserve time reversal symmetry (TRS). While pseudo magnetic fields couple to the Dirac fermions similarly to conventional magnetic fields and can produce Landau level (LL) quantization, they create a zero net magnetic flux at each lattice site. Therefore, electrons sitting at opposite points in the nodal line are related by TRS and must necessarily couple to opposite \mathbf{B} fields. In order to produce zero-field quantum Hall effect, one needs to create 3D LL quantization with well defined gaps in between. In 2D, the conventional Hall conductivity σ_{xy} is a dimensionless and quantized in units of e^2/h . In 3D, it has an extra unit of inverse length. According to Halperin [28], the Hall conductivity tensor is $\sigma_{ij} = e^2/(2\pi h) \epsilon_{ijk} G_k$, where \mathbf{G} is a reciprocal lattice vector (and could be zero). In general, a finite Hall conductivity in 2D (3D) is allowed whenever the chemical potential is in the gap between different LLs, and implies in the existence of chiral edge (surface) states. At zero field, the Hall conductivity tensor due to pseudomagnetic fields does not create chiral charge currents as in the conventional quantum Hall effect, but rather a valley current.

Strain engineering. In all possible strain configurations, the effective Hamiltonian (6) has the form $\mathcal{H}_p(\mathbf{q}) = h_1 \sigma_1 + h_2 \sigma_2$. In specific, for configuration

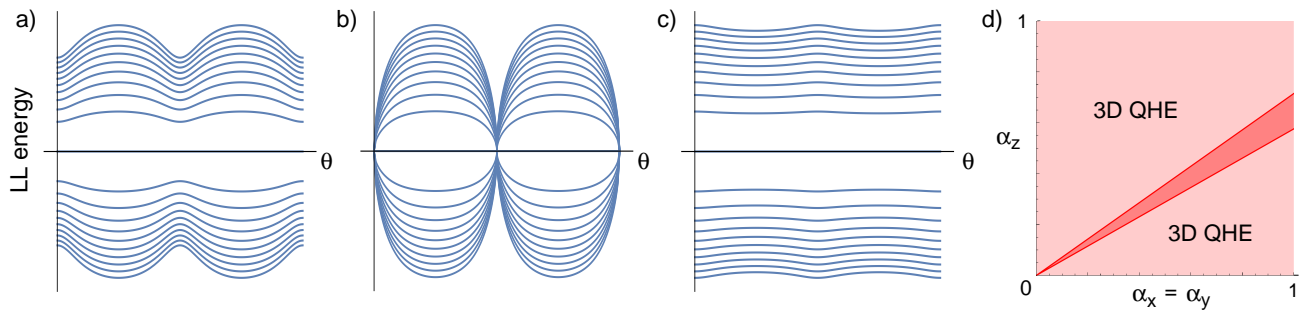


Figure 3. Energy of the Landau levels (LLs) around the nodal line vs. polar angle θ , ($0 \leq \theta < \pi$) for three strain configurations: (a) $\mathbf{u} = (2xz, 2yz, z^2)$, (b) $\mathbf{u} = (2yz, 2xz, 0)$ and (c) $\mathbf{u} = (2xz, 2yz, 0)$. The former and the latter configurations belong to a broader family of deformations $\mathbf{u} = (\alpha_x xz, \alpha_y yz, \alpha_z z^2)$ that produce nearly flat LLs in 3D. In (b), the LLs collapse at discrete points of the nodal line, preventing the zero-field QHE. Application of a uniform temperature gradient, $\Delta T \propto z$, creates strain fields in that family. (d) Phase space for $\alpha_x = \alpha_y$ and α_z with a zero-field 3D QHE (light red regions).

$$\mathbf{u} = (2xz, 2yz, z^2),$$

$$h_1 = v_x q_x + v_y q_y \quad (8)$$

$$h_2 = v_z q_z - \frac{\beta}{a} v_x x - \frac{\beta}{a} v_y y. \quad (9)$$

The corresponding pseudomagnetic field $\mathbf{B} = (-v_y/v_z, v_x/v_z, 0)$ forms a closed loop in the BZ around the nodal line, as shown in Fig. 2a. In order to calculate the spectrum of Landau levels, we generically define the canonically conjugated ladder operators $a = \frac{1}{\omega}(h_1 + ih_2)$ and $a^\dagger = \frac{1}{\omega}(h_1 - ih_2)$, which satisfy $[a, a^\dagger] = 2i[h_2, h_1]/\omega^2 = 1$. The parameter

$$\omega(s) = \sqrt{\frac{\beta}{a}} [2v_x^2(s) + 2v_y^2(s)]^{\frac{1}{2}}, \quad (10)$$

is the analog of the cyclotronic frequency. Taking the square of the Hamiltonian, $\mathcal{H}_0^2 = \omega^2 [a^\dagger a + \frac{1}{2}] 1_{2 \times 2} - \frac{1}{2} \omega^2 \sigma_3$, that results in the spectrum of LLs parametrized along the nodal line,

$$E_N(s) = \text{sgn}(N) \omega(s) \sqrt{|N|}, \quad (11)$$

with $N \in \mathbb{Z}$, as shown in Fig. 3a. The energy spectrum has a zeroth LL, as expected for Dirac fermions [1, 29], and a clear gap between the first few LLs. That permits the emergence of a zero-field QHE due to strain whenever the chemical potential lays in the LL gap. Even though there are many deformation sets producing uniform pseudomagnetic fields in real space, not all of them create 3D LL quantization with well defined gaps in between. For the strain configuration shown in Fig. 2b, $\mathbf{u} = (2yz, 2xz, 0)$, which corresponds to the pseudomagnetic field $\mathbf{B} = (-v_x/v_z, v_y/v_z, 0)$, the parameter $\omega(s) = \sqrt{(\beta/a)|v_x(s)v_y(s)|}$ has zeros along the nodal line (see Fig. 3b), where all LLs collapse. In that configuration, although the LLs are well defined away from those points, their dispersion does not lead to a well defined gap in the excitation spectrum, and hence the system does not have a zero-field QHE.

In general, one can define families of strain deformations that lead to a 3D zero-field QHE. While the energy spectrum is generically defined by Eq. (11), in those families $\omega(s) = \sqrt{2|[\hbar_2, \hbar_1]|}$ can be non zero for all points along the nodal line. For instance, one can build a family of strain deformations

$$\mathbf{u} = (\alpha_x xz, \alpha_y yz, \alpha_z z^2), \quad (12)$$

where the constants α_i ($i = x, y, z$) are such that $\omega(s) = \sqrt{(\beta/a)|\alpha_x v_x^2(s) + \alpha_y v_y^2(s) + \frac{3}{2}(\alpha_x + \alpha_y - 4\alpha_z)v_z^2(s)|}$ is non-zero for all s . The anisotropic case $\alpha_x = \alpha_y \gg \alpha_z$ is shown in Figure 3c. The phase space of parameters with $\alpha_x = \alpha_y$ that leads to a zero-field QHE is shown in the light red areas of Fig. 3d.

The deformation pattern $\mathbf{u} = (2xz, 2yz, 0)$ can be created with the strain forces indicated by the arrows in Fig. 4a. Interestingly, the physical implementation of the family of deformations (12) can be achieved with the application of a uniform temperature gradient along the z axis of the crystal (see Fig. 4b). Since \mathbf{u} describes the displacement of the lattice sites from their equilibrium position, the thermal expansion is represented as $u_i = \Delta x_i = x_i \gamma_i \Delta T \propto \gamma_i x_i z$, where $\gamma_i = dx_i/dT$ is the linear thermal expansion coefficient in the $i = x, y, z$ direction and $\Delta T(z) = T - T_0 \propto z$ is the temperature variation from equilibrium. This tunable pattern of deformations could be created with temperature gradients in crystals and acoustic metamaterials [19].

Elastic Hall viscosity. In quantum Hall systems, the Hall viscosity follows from the linear response of the system to gravitational fluctuations, which manifest through local changes in the metric of space $\xi_{ij} = \frac{1}{2}(\partial_i \xi_j + \partial_j \xi_i)$, where ξ_i has the physical meaning of a strain field. The so called gravitational Hall viscosity is defined as the variation of the stress tensor $T_{\mu\nu} = \partial \mathcal{H} / \partial \xi_{\mu\nu}$ to time variations of the strain tensor ξ_{ij} . By analogy, the elastic (phonon) Hall viscosity can be derived using linear re-

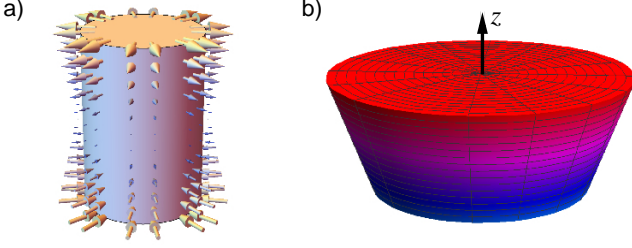


Figure 4. (a) Elastic deformation of a cylinder under the strain configuration $\mathbf{u} = (2xz, 2yz, 0)$. The arrows indicate the strain forces that create uniform nearly flat LLs in a 3D material (see fig. 3c). (b) Temperature gradient along the z axis that implements the strain field $\mathbf{u} = (\alpha_x xz, \alpha_y yz, \alpha_z z^2)$, with α_i ($i = x, y, z$) proportional to the thermal expansion coefficients. Red: hot region. Blue: cold.

sponse as [23–26]

$$\left\langle \frac{\partial \mathcal{H}_p}{\partial u_{\mu\nu}} \right\rangle = \lambda_{\mu\nu\rho\gamma} u_{\rho\gamma} + \eta_{\mu\nu\rho\gamma} \dot{u}_{\rho\gamma} \quad (13)$$

where $\langle \dots \rangle$ integrates over the fermions, $\lambda_{\mu\nu\rho\gamma}$ is the elastic moduli, $\dot{u}_{\rho\gamma}$ the strain-rate tensor and $\eta_{\mu\nu\rho\gamma}$ the elastic Hall viscosity tensor. The first term is the elastic response of a charge neutral fluid and the second one the viscous response [25, 26]. As the stress tensor, the tensors u , \dot{u} are symmetric, while the viscosity tensor is symmetric under $\mu \leftrightarrow \nu$ or $\rho \leftrightarrow \gamma$. However, with respect to the exchange $\mu\nu \leftrightarrow \rho\gamma$, the viscosity tensor has a symmetric part $\eta_{\mu\nu\rho\gamma}^S = \eta_{\rho\gamma\mu\nu}^S$ and an antisymmetric one $\eta_{\mu\nu\rho\gamma}^A = -\eta_{\rho\gamma\mu\nu}^A$. The symmetric part is associated with dissipation and vanishes at zero temperature. The antisymmetric one describes a non-dissipative response with topological nature and is non-zero only when TRS is broken. In general, one can calculate the antisymmetric viscosity tensor from the effective action

$$\delta S_H = \frac{1}{2} \int d^3x dt \eta_{\mu\nu\rho\gamma} u_{\mu\nu} \dot{u}_{\rho\gamma}, \quad (14)$$

which resembles a Chern-Simons action for the usual QHE [30, 31].

We will consider the elastic Hall viscosity for the 3D QAH state, which is an extension of the Haldane model for the hyperhoneycomb lattice, described in detail in ref. [20]. For nodal line semimetals, loop currents on the lattice can create a mass term around the nodal line with the general form

$$\mathcal{H}_m(\mathbf{q}) = \left[m(s) + \sum_{i=x,y,z} v'_i(s) q_i \right] \sigma_3, \quad (15)$$

where $v'_i(s)$ gives the mass dispersion in the $i = x, y, z$ direction. The Haldane mass $m(s)$ changes sign at $2(2n+1)$ points along the nodal line, with $n \in \mathbb{N}$, breaking inversion and TRS symmetry [20, 32]. The nodes of

the mass, where $m(s) = 0$, are Weyl points with a well defined helicity [20]. Weyl points with opposite helicities are connected by surface states in the form of topological Fermi arcs [33].

Effective action. In the QAH state, the Hamiltonian away from the Weyl points of the nodal line has the form

$$\mathcal{H}_{\text{QAH}}(\mathbf{q}) = \mathcal{H}_p(\mathbf{q}) + m(s)\sigma_3. \quad (16)$$

The effective action in terms of the strain tensor u_{ij} can be derived by integrating out the fermions. That results in the effective action $S_{\text{ef}}(u) = \text{Tr} [\ln(G^{-1})]$, where $G^{-1}(q) = iq_0 - \mathcal{H}_{\text{QAH}}(\mathbf{q}) \equiv G_0^{-1}(q) - \Sigma_{el}$ is the Green's function and

$$\Sigma_{el}(u) = v_z A_1 \sigma_1 + (v_x A_2 + v_y A'_2) \sigma_2 \quad (17)$$

is the self-energy due to elastic terms. For convenience, we defined the elastic gauge fields in (5) as $A_1 = -\frac{\beta}{a} \frac{3}{4} (u_{xx} + u_{yy} - 2u_{zz})$, $A_2 = -\frac{\beta}{a} u_{xz}$ and $A'_2 = -\frac{\beta}{a} u_{yz}$.

Expanding the action in powers of the elastic gauge fields, namely $S_{\text{ef}} = \text{tr} \ln G_0^{-1} - \text{tr} \sum_{n=0}^{\infty} \frac{1}{n} (G_0 \Sigma)^n$, the lowest order contribution to the Hall viscosity comes from two loop, $S_{\text{ef}}^{(2)} = -\frac{1}{2} \text{tr} [G_0 \Sigma G_0 \Sigma]$. More explicitly,

$$\delta S_{\text{ef}} = -\frac{1}{2} \int \frac{d^4k}{(2\pi)^4} [v_x v_z A_1(-k) \Pi^{12}(k) A_2(k) + v_y v_z A_1(-k) \Pi^{12}(k) A'_2(k) + (1 \leftrightarrow 2)], \quad (18)$$

where $\Pi^{\mu\nu}(k) = \int \frac{d^4q}{(2\pi)^4} \text{tr} [G_0(q+k) \sigma_\mu G_0(q) \sigma_\nu]$ is the standard polarization tensor, with antisymmetric off-diagonal terms, $\Pi^{12}(k) = -\Pi^{21}(k)$. Integration can be done by slicing the BZ into planes intersecting the nodal line at two points. Integrating over a slice in the xz plane for the first term,

$$v_x v_z \Pi^{12}(k) = \frac{k_0}{2\pi} \int_C \frac{dq_y}{(2\pi)} \nu_{(y)}(\mathbf{q}_0) = -\frac{k_0}{2\pi} \lambda_y, \quad (19)$$

where $\nu_{(y)}(\mathbf{k}_0) = \frac{1}{2} \text{sign}[v_x(s)v_z(s)m(s)] = \pm \frac{1}{2}$ is the topological charge of 2D massive Dirac fermions confined to an xz plane crossing the nodal line at \mathbf{k}_0 . Integration along the nodal loop C gives the y component of the Chern vector $\boldsymbol{\lambda} = (\lambda_x, \lambda_y, \lambda_z)$, which is belongs to the reciprocal lattice \mathbf{G} and sets the 3D quantum Hall conductivity of the system, $\sigma_{ij} = e^2/(2\pi h) \epsilon_{ijk} \lambda_k$. From a similar argument, $v_y v_z \Pi^{12}(k) = -v_y v_z \Pi^{21}(k) = k_0 \lambda_x/2\pi$. Hence,

$$\delta S_{\text{ef}} = \frac{1}{16\pi^2} \int \frac{d^4k}{(2\pi)^4} [-\lambda_x A_1(-k) k_0 A'_2(k) + \lambda_y A_1(-k) k_0 A_2(k) - (1 \leftrightarrow 2)]. \quad (20)$$

Performing the substitution $A_1 = d_z$, $A_2 = d_x$ and $A'_2 = d_y$, the effective action can be written in a more compact form,

$$\delta S_{\text{ef}} = \frac{1}{16\pi^2} \int d^4x \epsilon^{\mu\nu\rho} \lambda_\mu d_\nu \dot{d}_\rho, \quad (21)$$

where

$$\begin{aligned} d_x &= -\frac{\beta}{a}u_{xz}, \\ d_y &= -\frac{\beta}{a}u_{yz} \\ d_z &= -\frac{\beta}{a}\frac{3}{4}(u_{xx} + u_{yy} - 2u_{zz}). \end{aligned} \quad (22)$$

For the hyperhoneycomb lattice, the Chern vector is $\boldsymbol{\lambda} = \mathbf{b}_1 + \mathbf{b}_2 = (2\pi/\sqrt{3}, -2\pi/\sqrt{3}, 0)a^{-1}$ [20]. Writing the action in a more explicit form,

$$\delta S_{\text{ef}} = \frac{1}{2} \int d^4x \eta_H [(u_{xx} + u_{yy} - 2u_{zz})(\dot{u}_{yz} + \dot{u}_{xz}) - (u_{yz} + u_{xz})(\dot{u}_{xx} + \dot{u}_{yy} - 2\dot{u}_{zz})], \quad (23)$$

with $\eta_H = \beta^2\sqrt{3}/8\pi a^3$. The action can be cast in the form of (14), where the elastic Hall viscosity tensor is $\eta_{xxxx} = \eta_{xyxz} = \eta_{yyxz} = \eta_{yyyy} = \eta_H$, and $\eta_{zzxz} = \eta_{zzyz} = -2\eta_H$. The elastic Hall viscosity tensor is anisotropic, as expected in 3D [26], and reflects the topological nature of the QAH state [34]. In nodal-line semimetals, the Chern vector is related to the arclength separating two Weyls points *along* the nodal line. Hence, the shape of the nodal line contains information about the lattice and can be used even in effective low energy models to determine the *exact* elastic Hall viscosity in terms of the elastic parameter and lattice constant a .

Experimental observation. Although there are no known examples of semimetallic hyperhoneycomb crystals [35], this lattice may be artificially created in optical lattices [36], and also in photonic [4, 37] and acoustic metamaterials [19]. In twisted graphene bilayers, elastic gauge fields can be created with electric field effects [38]. In synthetic lattices, strain deformations can be readily implemented with local displacements of the lattice sites, without the need to apply pressure. While local probes

such as scanning tunneling spectroscopy can fully characterize the LLs in 2D [2, 3], this method can be used to characterize the surface states of the LLs in the 3D case.

In quantum Hall systems, the measurement of the Hall viscosity is typically challenging [39], as it involves probing the response of the stress tensor under changes of the space metric [26]. In Galilean invariant systems in the hydrodynamic regime, the Hall viscosity can be determined solely in terms of the electromagnetic response due to a non-homogeneous electric field [40, 41]. The elastic Hall viscosity nevertheless can be measured in terms of the dispersion of sound waves. When $\eta_H = \eta_{xxxx}$ is zero, the longitudinal and transverse modes are decoupled at long wavelengths. In the topological phase, where η_H is finite, the transverse and longitudinal modes are expected to mix, allowing one to measure the elastic Hall viscosity through the corrections to the dispersion of the phonons [23]. The quantum simulation of Chern insulating phases has been done in honeycomb lattices of cold atoms [36], in quantum circuits [42] and acoustic metamaterials [19]. We conjecture that the QAH state in 3D may be experimentally realized in synthetic lattices as well.

Conclusions. We have derived the elastic gauge fields that are created due to lattice deformations in the hyperhoneycomb lattice. We proposed a family of strain configurations that lead to uniform nearly flat LLs in 3D. The strain fields can be created with the application of uniform temperature gradient, driving a controllable reconstruction of the bulk states into nearly flat LLs. That raises the prospect of engineering tunable zero-field 3D QHE in metamaterials. In the topological phase, we have also shown that the components of the elastic Hall viscosity tensor in the 3D QAH state for this lattice are $\pm\eta_H$ or $\pm 2\eta_H$ (or zero), with $\eta_H = \beta^2\sqrt{3}/(8\pi a^3)$.

Acknowledgements. SWK thanks X. Dou for helpful discussions. BU and SWK acknowledge NSF CAREER grant No DMR-1352604 for support.

-
- [1] A. H. Castro Neto, N. M. R. Peres, F. Guinea, A. Geim, K. Novoselov, *Rev. Mod. Phys.* **81**, 109 (2009).
[2] N. Levy, S. A. Burke, K. L. Meaker, M. Panlasigui, A. Zettl, F. Guinea, A. H. Castro Neto, M. F. Crommie, *Science* **329**, 544 (2010).
[3] K. K. Gomes, W. Mar, Wonhee Ko, F. Guinea, H. C. Manoharan, *Nature* **483**, 306 (2012).
[4] M. C. Rechtsman, J. M. Zeuner, A. Tünnemann, S. Nolte, M. Segev and A. Szameit, *Nat. Photonics* **7**, 153 (2013).
[5] F. Guinea, M. I. Katsnelson and A. K. Geim, *Nat. Phys.* **6**, 30 (2010).
[6] L. Balicas, G. Kriza, and F. I. B. Williams, *Phys. Rev. Lett.* **75**, 2000 (1995).
[7] S. M. McKernan, S. T. Hannahs, U. M. Scheven, G. M. Danner, and P. M. Chaikin, *Phys. Rev. Lett.* **75**, 1630 (1995).
[8] B. A. Bernevig, T. L. Hughes, S. Raghu, and D. P. Arovas, *Phys. Rev. Lett.* **99**, 146804 (2007).
[9] D. Arovas and F. Guinea, *Phys. Rev. B* **78**, 245416 (2008).
[10] K. Mullen, B. Uchoa, and D. T. Glatzhofer, *Phys. Rev. Lett.* **115**, 026403 (2015).
[11] L.-K. Lim and R. Moessner, *Phys. Rev. Lett.* **118**, 016401 (2017).
[12] J.-W. Rhim and Y. B. Kim, *Phys. Rev. B* **92**, 045126 (2015).
[13] Y. Kim, B. J. Wieder, C. L. Kane, and A. M. Rappe, *Phys. Rev. Lett.* **115**, 036806 (2015).
[14] H. Weng, Y. Liang, Q. Xu, R. Yu, Z. Fang, X. Dai, and Y. Kawazoe, *Phys. Rev. B* **92**, 045108 (2015).
[15] R. Yu, H. Weng, Z. Fang, X. Dai, and X. Hu, *Phys. Rev. Lett.* **115**, 036807 (2015).
[16] T. T. Heikkilä and G. E. Volovik, *JETP Lett.* **93**, 59 (2011).
[17] Y. Chen, Y. Xie, S. A. Yang, H. Pan, F. Zhang, M. L.

- Cohen, and S. Zhang, *Nano Lett.* **15**, 6974 (2015).
- [18] L. S. Xie, L. M. Schoop, E. M. Seibel, Q. D. Gibson, W. Xie, and R. J. Cava, *APL Mater.* **3**, 083602 (2015).
- [19] Y. Zhu, Y. Peng, X. Fan, J. Yang, B. Liang, X. Zhu, J. Cheng, arXiv:1801.07942 (2018).
- [20] S. W. Kim, K. Seo, B. Uchoa, *Phys. Rev. B* **97**, 201101(R) (2018).
- [21] Frame effects can be accounted in higher order corrections in the derivative expansion. Those terms give geometrical corrections to the Hamiltonian, but do not affect the elastic gauge fields. See F. de Juan, J. L. Mañes, and M. A. H. Vozmediano, *Phys. Rev. B* **87**, 165131 (2013).
- [22] D. Haldane, *Phys. Rev. Lett.* **61**, 2015 (1988).
- [23] M. Barkeshli, S. Bum Chung, and X.-L. Qi, *Phys. Rev. B* **85**, 245107 (2012).
- [24] H. Shapourian, T. L. Hughes, and S. Ryu, *Phys. Rev. B* **92**, 165131 (2015).
- [25] J. E. Avron, R. Seiler, and P. G. Zograf, *Phys. Rev. Lett.* **75**, 697 (1995).
- [26] J. E. Avron, *J. Stat. Phys.* **92**, 543 (1998).
- [27] N. Read and E. Rezayi, *Phys. Rev. B* **84**, 085316 (2011).
- [28] B. I. Halperin, *Jpn. J. Appl. Phys.* **26**, 1913 (1987).
- [29] M. O. Goerbig, *Rev. Mod. Phys.* **83**, 1193 (2011).
- [30] T. L. Hughes, R. G. Leigh, and E. Fradkin, *Phys. Rev. Lett.* **107**, 075502 (2011).
- [31] A. Cortijo, Y. Ferreirós, K. Landsteiner, and M. A. H. Vozmediano, *Phys. Rev. Lett.* **115**, 177202 (2015).
- [32] R. Okugawa and S. Murakami, *Phys. Rev. B* **96**, 115201 (2017).
- [33] N. P. Armitage, E. J. Mele, and Ashvin Vishwanath, *Rev. Mod. Phys.* **90**, 015001 (2018).
- [34] A tilt in the nodal line breaks TRS and inversion symmetry, but preserves the product of the two, keeping the nodal line ungapped. This effect is not topological and does not lead by itself to a finite elastic Hall viscosity at zero temperature, even though it gives rise to a parity anomaly. In the presence of a small tilt angle in the QAH state, the nodal line breaks particle-hole symmetry around the Weyl points, inhibiting the topological response. See: H. Watanabe, Y. Hatsugai, and H. Aoki, *Phys. Rev. B* **82**, 241403(R) (2010); A. Martín-Ruiz and A. Cortijo, *Phys. Rev. B* **98** 155125 (2018).
- [35] K. A. Modic et al., *Nat. Commun.* **5**, 4203 (2014).
- [36] G. Jotzu, M. Messer, R. Desbuquois, M. Lebrat, T. Uehlinger, D. Greif, and T. Esslinger, *Nature (London)* **515**, 237 (2014).
- [37] L. Lu, L. Fu, J. D. Joannopoulos, and M. Soljačić, *Nat. Photonics* **7**, 294 (2013).
- [38] A. Ramires and J. L. Lado *Phys. Rev. Lett.* **121**, 146801 (2018).
- [39] A. I. Berdyugin, S. G. Xu, F. M. D. Pellegrino, R. Krishna Kumar, A. Principi, I. Torre, M. Ben Shalom, T. Taniguchi, K. Watanabe, I. V. Grigorieva, M. Polini, A. K. Geim, D. A. Bandurin, arXiv:1806.01606 (2018).
- [40] C. Hoyos, and D. T. Son, *Phys. Rev. Lett.* **108**, 066805 (2012).
- [41] F. D. M. Haldane, arXiv:0906.1854 (2009).
- [42] P. Roushan et al., *Nature (London)* **515**, 241 (2014).